Published in final edited form as:
Mol Cell. 2012 February 10; 45(3): 330–343. doi:10.1016/j.molcel.2011.11.032.

Direct Recruitment of Polycomb Repressive Complex 1 (PRC1) to Chromatin by Core Binding Transcription Factors

Ming Yu[1,2,3], **Tali Mazor**[2,4,5], **Hui Huang**[1], **Hsuan-Ting Huang**[1], **Katie L. Kathrein**[1], **Andrew J. Woo**[1], **Candace R. Chouinard**[4,5], **Adam Labadorf**[4,5], **Thomas E. Akie**[1], **Tyler B. Moran**[1], **Huafeng Xie**[1], **Sima Zacharek**[1], **Ichiro Taniuchi**[6], **Robert G. Roeder**[7], **Carla F. Kim**[1,8], **Leonard I. Zon**[1,8,9], **Ernest Fraenkel**[4,5,10], and **Alan B. Cantor**[1,8,11]

[1]Children's Hospital Boston and Dana-Farber Cancer Institute, Harvard Medical School, Boston, MA, USA 02115

[4]Department of Biological Engineering, Massachusetts Institute of Technology, Cambridge, MA, USA 02139

[5]Computer Science and Artificial Intelligence Laboratory, Massachusetts Institute of Technology, Cambridge, MA, USA 02139

[6]Laboratory for Transcriptional Regulation, Research Center for Allergy and Immunology, RIKEN, Yokohoma, Kanagawa, Japan

[7]Laboratory of Biochemistry and Molecular Biology, The Rockefeller University, New York, NY, USA 10065

[8]Harvard Stem Cell Institute, Cambridge, MA, USA 02138

[9]Howard Hughes Medical Institute, Boston, MA, USA 02115

Summary

Polycomb repressive complexes (PRCs) play key roles in developmental epigenetic regulation. Yet the mechanisms that target PRCs to specific loci in mammalian cells remain incompletely understood. In this study, we show that Bmi1, a core component of Polycomb Repressive Complex 1 (PRC1), binds directly to the Runx1/CBFβ transcription factor complex. Genome-wide studies in megakaryocytic cells demonstrate significant chromatin occupancy overlap between the PRC1 core component Ring1b and Runx1/CBFβ, and functional regulation of a considerable fraction of commonly bound genes. Bmi1/Ring1b and Runx1/CBFβ deficiency generate partial phenocopies of one another *in vivo*. We also show that Ring1b occupies key Runx1 binding sites in primary murine thymocytes and that this occurs via Polycomb Repressive Complex 2 (PRC2) independent mechanisms. Genetic depletion of Runx1 results in reduced Ring1b binding at these sites *in vivo*. These findings provide evidence for site-specific PRC1 chromatin recruitment by core binding transcription factors in mammalian cells.

[10]Corresponding Author: 77 Massachusetts Ave. Building 68, Room 323A Cambridge, MA 02139 fraenkel-admin@mit.edu.
[11]Corresponding Author: 300 Longwood Ave., Karp 7 Children's Hospital Boston Boston, MA 02115 Tel: 617-919-2026 Fax: 617-730-0222 alan.cantor@childrens.harvard.edu.
[2]Authors contributed equally.
[3]Current address: Laboratory of Biochemistry and Molecular Biology, The Rockefeller University, New York, NY, USA 10065

Introduction

Polycomb group (PcG) proteins were first identified in homeotic transformation screens in *Drosophila melanogaster* through their silencing of homeobox (Hox) genes (for review, see (Simon and Kingston, 2009)). They are now known to developmentally regulate a large number of genes, and play key roles in mammalian stem cell self-renewal, cellular differentiation and neoplasia. Two phylogenetically conserved PcG complexes have been identified: Polycomb Repressive Complex 1 and 2 (PRC1 and PRC2). PRC1 is composed of the core proteins Bmi1 (also called Pcgf4) and Ring1b, and a variable number of associated components such as Ring1a, CBX proteins, PH1, PH2, and other Pcgf proteins in mammals. It silences genes through histone 2A monoubiquitination (H2Aub) and/or nucleosome compaction. Bmi1 and Ring1b deficient animals have hematopoietic, neurologic and skeletal defects, and develop stem cell exhaustion due to impaired stem cell self-renewal (Cales et al., 2008; Park et al., 2003; van der Lugt et al., 1994). PRC2 contains the core components EZH2, Suz12 and EED, and is also implicated in stem cell maintenance and lymphocyte homeostasis (Margueron and Reinberg, 2011). It catalyzes the methylation of histone 3 at lysine 27 (H3K27me).

As PRCs do not contain inherent DNA-specific binding activity, additional factors must mediate their site-specific chromatin recruitment. In *Drosophila*, DNA polycomb response elements (PREs) and targeting factors have been defined. However, site-specific targeting mechanisms in mammalian cells remain less well understood.

Core binding transcription factors are heterodimeric complexes composed of a common CBFβ subunit bound to one of three tissue-specific DNA-binding CBFα subunits (now called Runx1,-2,-3). Like PRCs, core binding transcription factors play roles in stem cell self-renewal, tissue differentiation, and cancer (for review, see (Appleford and Woollard, 2009)). Runx1 is the predominant hematopoietic expressed CBFα family member, whereas Runx2 and Runx3 play roles in bone and neural development. Targeted disruption of *Runx1* in mice leads to complete failure of definitive hematopoiesis during embryogenesis due to defective emergence of the first definitive hematopoietic stem cells (HSCs) from the aorto-gonadal-mesonephros (AGM) region (Chen et al., 2009; Kissa and Herbomel, 2010; North et al., 1999; Wang et al., 1996a). In adult mice, inducible Runx1 deficiency results in blocked megakaryocyte (Mk) maturation, impaired lymphopoiesis, myeloid cell hyperproliferation, and progressive HSC exhaustion (Growney et al., 2005; Ichikawa et al., 2004; Jacob et al., 2010; Sun and Downing, 2004). Similar defects are seen with CBFβ deficiency (Talebian et al., 2007; Wang et al., 1996b).

Runx1 and *CBF*β are the most common targets of genetic alteration in human leukemia, occurring in about ~20–25% of all cases (Speck and Gilliland, 2002). *Runx1* is also mutated in a subset of myelodysplastic syndrome (MDS), and is associated with poor prognosis (Bejar et al., 2011). Germline *Runx1* haploinsufficiency causes familial thrombocytopenia, platelet dysfunction, and increased MDS/leukemia risk (Song et al., 1999).

In order to further understand Runx1 transcriptional mechanisms, we recently purified Runx1 containing multiprotein complexes from megakaryocytic cells (Huang et al., 2009). Here, we report the direct physical and functional association between Runx1/CBFβ and PRC1. Moreover, we provide evidence that Runx1 recruits PRC1 directly to chromatin in a PRC2 independent manner. These findings support a mechanism of site-specific PRC1 chromatin recruitment in mammalian cells, and conversely implicate a role for PRC1 in core binding factor mediated gene regulation.

Results

Runx1/CBFβ interact with PRC1 in megakaryocytic and T-lymphocytic cells

We previously purified Runx1 containing multiprotein complexes from 12-*O*-tetradecanoylphorbol-13-acetate (TPA)-induced murine L8057 megakaryoblastic cells using metabolic biotin tagging and streptavidin (SA) affinity chromatography, and identified associated proteins by liquid chromatography coupled to tandem mass spectrometry (LC/MS/MS) (Huang et al., 2009). In addition to known interacting proteins such as CBFβ GATA-1, GATA-2, TAL1/SCL, Sin3A, PRMT1, PML, Smad2, CDK6, and the SWI/SNF complex, we identified physical and functional interactions between Runx1 and the ets transcription factor FLI1 (Huang et al., 2009). From these same preparations, we obtained multiple components of Polycomb Repressive Complex 1 (PRC1) and TrxG chromatin-remodeling complexes (Figure 1A, Supplemental Figure S1, Supplemental Table S1). Physical association between FLAG tagged and biotinylated-Runx1 ($^{FLAG\text{-}Bio}$Runx1) and the PRC1 core components Ring1b and Bmi1 was confirmed by Western blot from independent SA pull-down experiments (Figure 1B). The abundant Mk nuclear protein YAP was not detected, indicating specificity of the assay. No significant difference in interactions was noted using uninduced or TPA-induced L8057 cells (Supplemental Figure S2). Physical association between CBFβ/Runx1 and Ring1b/Bmi1 was further validated by co-immunoprecipitation (co-IP) assays of endogenous proteins in both directions (Figures1C–E). Physical interaction between CBFβ and Ring1b/Bmi1 was also observed in human Jurkat T cells (Fig. 1F). Glutathione-s-transferase (GST) pull-down assays using purified recombinant proteins show that Runx1 and Bmi1 interact directly, and that the runt domain of Runx1 is sufficient for Bmi1 binding (Fig. 1G). Additional mapping studies indicate that a region involving amino acids 1–57 of Bmi1, which largely contains the Ring domain, contributes significantly to Runx1 binding, although sequences from amino acids 57–167 also participate (Figure 1H).

Runx1/CBFβ and Ring1b occupy a large number of common chromatin sites in L8057 cells

To assess the association of Runx1/CBFβ and PRC1 at the chromatin level, chromatin immunoprecipitation-high throughput sequencing (ChIP-seq) was performed for Runx1, CBFβ, and Ring1b in TPA-induced L8057 cells. High-quality Bmi1 antibodies are not available for ChIP-seq. Two biological repeats were performed for each, and the data was compared to control IgG. After aligning sequences to the genome and removing redundant reads and those that mapped to multiple locations, we obtained 44,532,375 filtered reads for Runx1, 48,623,085 for CBFβ and 56,381,939 for Ring1b (Supplementary Table S2). This corresponds to a total of 7,073 Runx1, 10,186 CBFβ, and 7,063 Ring1b peaks (p-value <1E–10 and false discovery rate (FDR) < 5%) using the peak-calling algorithm MACS (Zhang et al., 2008); and 5,595 Runx1, 6,685 CBFβ, and 4,239 Ring1b genes bound between −1kb upstream of the transcription start site (TSS) to +1kb downstream of the transcription end site (TES) (see Supplemental Figure S3A for gene calls using a −10 kb to + 10 kb window). As expected, there was considerable overlap between Runx1 and CBFβ occupancy peaks (Figure 2A). Seventy-nine percent of the Runx1 peaks were bound by CBFβ, and 55% of the CBFβ peaks were bound by Runx1. There was also significant overlap of Runx1/CBFβ and Ring1b peaks. Fifty-seven percent of the Runx1 peaks were bound by Ring1b, and 57% of the Ring1b peaks were bound by Runx1. Forty-eight percent of the CBFβ peaks were bound by Ring1b, and 70% of the Ring1b peaks were bound by CBFβ. Three thousand six hundred and eighty-eight peaks and 3,097 genes were common to all three factors.

To analyze whether Ring1b was binding at the same sites as Runx1 and CBFβ, we used the Genome Positioning System (GPS) algorithm (Guo et al., 2010), which overcomes the low resolution of ChIP-Seq experiments arising from random DNA fragmentation. Using this

method, we found that 61% of Ring1b binding sites have a binding site for CBFβ or Runx1 within 100 bp (Figure 2B).

Examples of gene loci bound by all 3 factors are shown in Fig. 2C (see Supplemental Figure S3B for additional loci). The high degree of common occupancy between Ring1b and Runx was confirmed using a second Ring1b antibody (Supplemental Figure S4A). Quantitative ChIP (qChIP) assays from independent samples validated commonly occupied peaks for 27 of 28 sites tested (Figure 2D). Each of two sites assayed in purified murine fetal liver derived Mks also show occupancy by both CBFβ and Ring1b (Figure 2E).

ChIP-seq experiments carried out in uninduced L8057 cells also showed a high degree of overlap between Runx1, CBFβ and Ring1b bound sites, although the total numbers of peaks (3,310 Runx1, 6,158 CBFβ, and 6,628 Ring1b) and bound genes (2,526 Runx1, 4,385 CBFβ, and 4,130 Ring1b) were lower than that observed for the induced cells (Supplemental Figure S4B). A total of 2,070 peaks and 1,710 genes were bound by all 3 factors.

As expected, transcription factor binding motif analysis under Runx1 and CBFβ occupancy peaks showed enrichment for the Runx consensus binding sequence (g.w.ACCACAra) (p= 2.9E-71 and p=1.2E-54, respectively) (Supplemental Table S3). Motifs corresponding to Ets and GATA family transcription factors, which physically and functionally interact with Runx proteins (Elagib et al., 2003; Huang et al., 2009; Kim et al., 1999; Wilson et al., 2010), were also highly enriched. Ring1b occupancy sites were likewise enriched for Runx1 (p=7.9E-13), Ets (p=2.1E-65), and GATA (p=6.8E-18) binding sequences.

Ring1b and CBFβ regulate a subset of commonly bound genes in Mks

In order to correlate chromatin occupancy with functional gene regulation, CBFβ and Ring1b lentiviral shRNA knock down was performed in TPA-induced L8057 cells, and gene expression changes were measured by cDNA microarray analysis. A previously characterized CBFβ shRNA construct (Galli et al., 2009) produced marked reduction of CBFβ protein levels (Figure 3A). Runx1 and Ring1b levels were not significantly affected. From 3 independent experiments, a total of 874 genes changed expression ≥ 1.5-fold with a p-value <0.05, compared to the empty vector. Five hundred and ninety-five genes were up regulated and 279 were down regulated. *CBF*β was the most down regulated gene, whereas *Ring1b* and *Bmi1* were not significantly altered. Among the 2,782 genes bound by all 3 factors (Runx1, CBFβ, and Ring1b) (p-value 1E-10, FDR <5%, binding −1kb from TSS to +1kb from TES) and represented by probes on the array that passed quality control, 280 genes changed expression. Two hundred and seventeen were up regulated (p-value 3.4E-46) and 63 were down regulated (p-value 2.9E-5). As distal binding events strongly influence gene expression (MacIsaac et al., 2010), we repeated these calculations including genes bound from −10kb from TSS to +1kb from TES. Among the 3,530 genes bound by all 3 factors (p-value 1E-10, FDR <5%), 341 genes changed expression. Two hundred and sixty two were up regulated (p-value 4.0E-54) and 79 were down regulated (p-value 2.7E-6). Genes that were bound in multiple regions and those bound only in the distal promoter, introns or exons were associated with up regulation (Supplemental Table S4). Bound and up regulated genes were enriched for intracellular signaling (Benjamini p-value 0.009), regulation of biological process (p-value 0.02), signal transduction (p-value 0.02), biological regulation (p-value .02), and regulation of cellular process (p-value 0.03) (Dennis et al., 2003).

Although knockdown for Ring1b was not as efficient as that for CBFβ, the more potent shRNA construct (shRNA #1) produced significant Ring1b protein reduction (Figure 3B). Runx1 and CBFβ protein levels were not significantly altered. A total of 497 genes changed expression ≥ 1.5 fold with a p-value <0.05. One hundred and fifty-two genes were up

regulated and 345 were down regulated. Among the 3,530 genes bound by all 3 factors and represented by probes on the array, 65 were up regulated (p-value 1.5E-13) and 99 were down regulated (p-value 8.3E-8).

Clustering analysis of genes occupied by either Runx1, CBFβ and/or Ring1b within −1kb of the TSS to +1kb of the TES, and a heat map of corresponding gene expression changes following CBFβ or Ring1b shRNA knock down are shown in Figure 3C (see Supplemental Figure S5 for comparable analysis based on binding −10 kb of TSS to +1 kb of TES). Fifty-one genes that were bound by all 3 factors changed expression with both CBFb and Ring1b shRNA knock down using the high stringency criteria described above (Supplemental Table S5). Eighty-eight percent of the genes changed expression in the same direction (28 genes up regulated, 17 down regulated) (Figure 3D). qRT-PCR validation studies from independent experiments confirmed the gene expression changes in representatives of each of these classes (Figure 3E). We conclude that CBFβ/Runx1 and Ring1b functionally regulate a set of commonly bound genes.

Deficiency of Ring1b and Bmi1 impairs Mk maturation

Runx1 or CBFβ deficiency impairs Mk maturation as evidenced by reduced ploidy and poor platelet production (Growney et al., 2005; Ichikawa et al., 2004; Talebian et al., 2007). To examine the functional role of Ring1b in Mk maturation, we measured the ability of L8057 Ring1b shRNA knock down cells to undergo TPA-induced endomitosis. As shown in Figure 4A, Ring1b knock down resulted in reduced ploidy (mean 2.8N ± 0.7 (n=4) compared to the empty vector control (4.5N ± 1.3 (n=5)), and was similar to that observed with CBFβ knock down (mean ploidy 2.5N ± 0.5 (n=3)).

Bmi1$^{-/-}$ neonatal mice are thrombocytopenic (and lymphopenic), but have normal hemoglobin and granulocyte levels (Park et al., 2003). To probe for a potential Mk defect in these animals, we examined bone marrow histology and cultured Mks from 5–6 week old Bmi1$^{-/-}$ mice. This showed that Bmi1$^{-/-}$ Mks were smaller in size, contained more hypolobulated nuclei, and had reduced ploidy compared to Bmi1$^{+/-}$ littermates (Figure 4B). This is similar to the phenotype of Runx1 deficient Mks (Growney et al., 2005; Ichikawa et al., 2004). These findings are consistent with functional overlap of Runx1/CBFβ and Ring1b/Bmi1 in Mk maturation.

Morpholino knock down of Bmi1 or Ring1b impairs HSC development in zebrafish embryos

Deficiency of either Runx1 or Bmi1/Ring1b leads to HSC exhaustion in adult animals. Runx1/CBFβ deficiency also causes defects in definitive HSC ontogeny during embryogenesis. However, a detailed examination Bmi1/Ring1b's role in embryonic HSC ontogeny has not been reported to our knowledge. In order to examine this, we knocked down their expression using morpholinos (MOs) in zebrafish embryos. The first definitive HSCs develop in the equivalent AGM region of the developing zebrafish embryo at about 36 hrs post fertilization (hpf), and are marked by expression of c-Myb and/or Runx1 (Burns et al., 2002). As previously reported (Burns et al., 2005), Runx1 MO knock down ablated phenotypic (c-Myb^{+}) definitive HSC formation (Fig. 5A, left panel). MO knockdown of Bmi1 and the duplicated zebrafish gene Bmi1b, or Ring1b also resulted in loss of c-Myb^{+}/Runx1^{+}cells, although not to as full an extent as Runx1 knock down (Figure 5A, right panel).

As a complementary approach, knock down experiments were performed in CD41-eGFP transgenic fish, which express eGFP in HSC/early progenitor cells (HSPCs) and thrombocytes (Lin et al., 2005). Like Runx1, knock down of Bmi1/Bmi1b and Ring1b

resulted in a significant reduction of $eGFP^+$ cells in the AGM region, as well as in the caudal hematopoietic tissue (CHT), which is seeded by AGM HSCs (Figure 5B). Similar to Runx1 deficiency (Wang et al., 1996a), Bmi1/Bmi1b or Ring1b knock down did not significantly affect primitive erythropoiesis (Figure 5C), or alter overall morphology of the embryos (Supplemental Figure S6).

Both Bmi1 and Runx1 knock out mice have a block in T cell maturation at the $CD4^-CD8^-$ double negative (DN) to $CD4^+CD8^+$ double positive (DP) transition stage, although Bmi1 loss predominantly impairs the DN3 ($CD44^-CD25^+$) to DN4 transition ($CD44^-CD25^-$) (Miyazaki et al. 2008) whereas Runx1 loss predominantly impairs the DN2 ($CD44^+CD25^+$) to DN3 transition (Ichikawa et al., 2004). Thus, like in Mk development and HSC ontogeny, Ring1b/Bmi1 or Runx1/CBFβ deficiencies generate partial phenocopies of one another with respect to T-lymphocyte development. In total, these findings argue for functional cooperation between Runx1 and PRC1 components in development.

Runx1 recruits Ring1b to Runx1 binding sites in primary murine thymocytes

To examine whether Runx1 participates in Ring1b recruitment at selected chromatin sites, we performed qChIP assays for Runx1, CBFβ, and Ring1b in primary thymocytes from $Runx1^{fl/fl}$,Vav1-Cre mice, which have pan-hematopoietic deletion of Runx1 (Chen et al., 2009). In control mice ($Runx1^{fl/fl}$), we observed significant enrichment for Runx1 and CBFβ at the previously described Runx1 binding sites in the *CD4* silencer (Yu et al., 2008), *Th-POK* regulatory regions (Th-POK RBS1 and 2) (Setoguchi et al., 2008), and *TCR*b enhancer (Setoguchi et al., 2008), as well as several sites inferred from our Mk ChIP-seq dataset (*Top2b*, *Stat1*, and *Stat3* promoters) (Figure 6A). Only low levels of Runx1/CBFβ were found at the Th-POK promoter, consistent with our previous report (Setoguchi et al., 2008). Ring1b was significantly enriched at each of the Runx1/CBFβ occupied sites.

In the knock out mice, Runx1 and CBFβ enrichment were markedly reduced at these sites, as expected (Figure 6A). Low levels of residual Runx1 are likely due to incomplete conditional allele excision. Importantly, Ring1b is also markedly depleted at these sites. H2Aub enrichment was found at a subset of Runx1, CBFβ, and Ring1b commonly occupied sites in control mice, and was also markedly depleted upon Runx1 deletion (Figure 6B). Control experiments validated the chromatin integrity of the knock out animal samples (Supplemental Figure S7).

To examine these effects in a more global manner, we performed ChIP-seq for Runx1, CBFβ and Ring1b in primary thymocytes from $Runx1^{fl/fl}$ and $Runx1^{fl/fl}$, Vav1-Cre 5–8 week old mice. From the $Runx1^{fl/fl}$ mice, we obtained 1,898,522 Runx1, 2,109,935 CBFβ, and 1,543,887 Ring1b aligned and filtered reads (Supplementary Table S2). This corresponds to 1,507 Runx1, 4,033 CBFβ, and 712 Ring1b peaks (p-value <E-10, FDR<5%), and 1,364 Runx1, 3,369 CBFβ, and 665 Ring1b bound genes (binding between −1kb of TSS to +1 kb of TES). Similar to our findings in L8057 cells, there was considerable overlap of the occupancy peaks and genes of all 3 factors (Figure 6C). Forty-six percent of the Ring1b bound genes were also bound by Runx1, and 71% were bound by CBFβ. Two hundred and ninety-two genes were bound by all 3 factors (Supplemental Table S6).

From the $Runx1^{fl/fl}$, Vav1-Cre mice, we obtained 1,597,571 Runx1, 2,571,167 CBFβ, and 2,197,463 Ring1b aligned and filtered reads (Supplementary Table S2). None of the Runx1 or CBFβ peaks met the statistical cut-off of a p-value of <1E–10, and FDR<5%. Although 23 Ring1b peaks remained in the Runx1 deficient thymocytes, only one of these corresponds to a Runx1/CBFβ commonly bound site from the control mice. A more detailed analysis of the binding data revealed that even in the Runx1 knock out animals some residual Runx1

binding could be detected, reflecting incomplete excision of the floxed allele. To quantify this, we counted the number of unique reads associated with peaks bound by all three proteins in the control animal and at the same loci in the knock out animal (Figure 6D). For Ring1b, 7% of the regions had no reads at all in the knock out animals (compared to 8% for Runx1 and 2% for CBFβ). At the remaining sites, the median ratio of reads at these locations in the control to knock out was 4.1 for Runx1, 5.2 for CBFβ, and 1.3 for Ring1b. The reduced read numbers in the Runx1 deficient thymocytes occurs despite the fact that the libraries for Ring1b and CBFβ were sequenced more deeply in these mice. (The expected ratios based on the number of uniquely mapped reads would be 1.2 for Runx1, 0.8 for CBFβ and 0.7 for Ring1b). Examples of ChIP-seq profiles showing the concomitant decrease in Runx1, CBFβ, and Ring1b reads upon Runx1 depletion are shown in Figure 6E. We conclude that Runx1/CBFβ participates in Ring1b recruitment at some commonly bound sites.

To examine the possibility that PRC1 may recruit or stabilize Runx1, qChIP assays were performed from primary thymocytes of 5–6 week old $Bmi1^{-/-}$ mice. With the exception of the TOP2b promoter, we observed no significant difference of Runx1 enrichment at the sites tested (Figure 6F). These data are consistent with Runx1 mediated recruitment of PRC1, rather than PRC1 mediated recruitment or stabilization of Runx1.

Ring1b occupancy at commonly bound Runx1/CBFβ sites occurs independent of PRC2

A proposed model of PRC1 chromatin recruitment involves its direct binding to H3K27me3 residues, which are first generated by the action of PRC2 (Simon and Kingston, 2009). In order to examine whether H2K7me3 is involved in PRC1 recruitment at Runx1/CBFβ commonly occupied sites, we measured H3K27me3 enrichment levels at each of the tested sites in wild type primary thymocytes. Although significant H3K27me3 enrichment was observed at the Th-POK RBS1, RBS2 and promoter regions, all of the other sites had only background levels (Figure 7A).

To test this further, we examined Runx1, CBFβ and Ring1b chromatin occupancy in thymocytes from $EZH2^{fl/fl}$,Vav1-Cre, Rosa26-flox-stopper-flox-EYFP mice (Wilson et al., 2011). Flow cytometry of thymocytes and splenocytes show that 91.2 % and 95.9% of the total cells express EYFP, respectively, indicating efficient activation of Cre in these tissues. Of the $CD3^{+}$ populations (T-cells), 96.3% and 98.4% were EYFP positive and had 12 and 29-fold decreases in EZH2 mRNA levels compared to control mice for spleen and thymus, respectively (Figure 7B). Despite this marked EZH2 depletion, qChIP assays from the thymocytes of these animals demonstrated no significant loss of Ring1b, Runx1 or CBFβ chromatin occupancy at the sites tested (Figure 7C). This strongly suggests that recruitment of Ring1b to these Runx1/CBFβ occupied sites occurs independent of PRC2 activity.

Discussion

In this study, we provide evidence that core binding transcription factors contribute to site-selective physical and functional recruitment of PRC1 in mammalian cells. In *Drosophila*, polycomb response elements (PREs) have been defined based on functional assays, and consist of several hundred base pair sequences (Simon and Kingston, 2009). These regions contain binding sites for the transcription factor PHO (orthologue of the mammalian transcription factor YY1), which participates in PcG recruitment in some cases. Less is known about PcG recruitment in mammalian cells. Several examples of non-coding RNA mediated recruitment have been uncovered, particularly in X-chromosome inactivation (Zhao et al., 2008). Woo et al. recently defined a PRC recruitment site within the human HOXD cluster (Woo et al., 2010). We recently showed that the lineage-specific transcription factor GATA-1 physically and functionally associates with PRC2 during erythroid terminal

maturation (Yu et al., 2009). The findings in the current study indicate that Runx1 and CBFβ contribute to direct PRC1 recruitment at some sites in Mks and lymphocytes. It is of interest to note that both YY1 and Runx factors share a common central TGG core element in their DNA consensus binding sites.

There is prior evidence that PRC1 can be recruited to chromatin independent of PRC2 (Pasini et al., 2007; Schoeftner et al., 2006; Vincenz and Kerppola, 2008). Our data are consistent with the existence of PRC2 independent mechanisms, and suggest that direct interactions with DNA-binding proteins, such as core binding transcription factors, may be responsible in some cases. Similar to our findings, direct interaction between PRC1 and PHO has been described in *Drosophila* (Mohd-Sarip et al., 2006).

Like many transcription factors, Runx proteins both activate and repress transcription in a gene and developmental context-dependent manner. For example, Runx1 activates the *PU.1* gene in myeloid and B cells, but represses it in T-lymphocytes and Mks (Huang et al., 2008). Some Runx associated repressive events are mediated by Groucho/TLE family proteins. However, there is also evidence that Groucho-independent mechanisms exist (Walrad et al., 2011). The findings from the current study suggest that PRC1 may be involved in some of these alternate repressive pathways.

Genetic suppressor screens in *Drosophila* indicate that SWI/SNF and TrxG chromatin remodeling factors play antagonistic roles to PcG mediated gene silencing (Simon and Kingston, 2009). Interestingly, we identified multiple components of the SWI/SNF and TrxG (ASH2/SET complex) complexes in our Runx1 multiprotein complex purifications. Bakshi et al. recently reported that SWI/SNF physically interacts with Runx1 and controls hematopoietic target genes (Bakshi et al., 2010). Moreover, they showed that reduced Runx1 levels correlate with impaired SWI/SNF chromatin occupancy at several common loci. Collectively, these findings suggest that Runx proteins may differentially recruit PcG and SWI-SNF/TrxG complexes in a gene- and developmental specific context.

Adult HSC self-renewal is impaired in both Bmi1/Ring1b and Runx1 deficient animals (Cales et al., 2008; Jacob et al., 2010; Park et al., 2003; Sun and Downing, 2004; van der Lugt et al., 1994). Our data in zebrafish embryos indicate that Ring1b and Bmi1, like Runx1/CBFβ, are also involved in definitive HSC ontogeny (Figure 5). However, the fact that Bmi1$^{-/-}$mice (Park et al., 2003; van der Lugt et al., 1994) lack the complete failure of HSC development seen in Runx1$^{-/-}$ mouse embryos (Wang et al., 1996a) indicates that either PRC1 is not absolutely required for Runx1 function in HSC ontogeny, and/or that compensatory mechanisms exist. Runx1 is also an upstream regulator of *Bmi1* in HSCs (Motoda et al., 2007), which could explain some of the HSC phenotypic overlap.

How dysregulation of Runx proteins predisposes to cancer is not fully understood. All of the human leukemia associated *Runx1* chromosomal translocations generate fusion proteins that retain the runt domain. Moreover, many malignancy-related *Runx1* somatic and germline point mutations affect the runt domain. It will be of interest to determine if any of these abnormal products lead to altered PRC1 chromatin recruitment and epigenetic changes, and whether this plays a role in Runx1 related malignancies.

In summary, the data presented in this study provide evidence that core binding transcription factors contribute to chromatin recruitment of PRC1 at site-specific loci in megakaryocytic and lymphocytic cells. Future studies will be needed to determine if other lineage-specific transcription factors also play a direct role in recruiting PRC1 in different tissue contexts.

Experimental Procedures

See Supplemental Experimental Procedures for more details.

Cells and cell culture

The L8057-*birA* and L8057-$^{FLAG\text{-}bio}$Runx-1 cell lines were generated and cultured as previously described (Huang et al., 2009). Cell maturation was induced by adding 50 nM (final concentration) 12-*O*-tetradecanoylphorbol-13-acetate (TPA) to the medium for 3 days.

Conditional knock out mice

Runx1$^{fl/fl}$ mice were kindly provided by D. Gary Gilliland (Growney et al., 2005), and interbred with Vav1-Cre mice (Georgiades et al., 2002). EZH2$^{fl/fl}$, flox-stopper-flox Rosa26-EYFP, Vav1-Cre mice (Wilson et al., 2011) were kindly provided by Stuart Orkin. Bmi1$^{-/-}$ mice were kindly provided by Maarten van Lohuizen (van der Lugt et al., 1994).

Runx1 multiprotein complex purification and proteomic analysis

Runx1 containing multiprotein complexes were purified and characterized as previously described (Huang et al., 2009). Co-purified proteins were separated by sodium dodecyl sulfate polyacrylamide electropheresis (SDS-PAGE), and the entire lane was analyzed by liquid chromatography coupled to tandem mass spectrometry using an LTQ linear ion-trap mass spectrometer (Thermo Scientific). Peptide sequences were determined by matching protein or translated nucleotide databases with the acquired fragmentation pattern by the software program SEQUEST (Thermo Scientific) (Eng, 1994).

Co-immunoprecipitation (Co-IP) assays

Co-IP assays were performed as previously described (Yu et al., 2009). See Supplemental Experimental Procedures for more details.

Glutathione-s-transferase (GST) pull-down assays

See Supplemental Experimental Procedures.

Chromatin immunoprecipitation (ChIP) and ChIP-sequencing (ChIP-seq)

Cells were fixed with 0.4% formaldehyde at room temperature for 10 min. For primary Mk studies, fetal liver cells were harvested from embryonic day 13.5 C57BL/6 murine embryos, cultured in the present of 1% thrombopoietin (Tpo) conditioned medium (Villeval et al., 1997) for 4 days, and mature Mks were enriched by discontinuous bovine serum albumin density gradient as previously described (Drachman et al., 1997). For primary thymocyte studies, whole thymuses from 5–8 week old mice were dissected, and single cell suspensions were generated by gentle grinding of the tissue and passage through a 100 μM cell strainer in RPMI 1640 medium containing 10% heat inactivated fetal calf serum. Thymocytes were cross-linked with 1% formaldehyde (final conc.) for 5 min at room temperature.

qChIP assays were performed as previously described (Yu et al., 2009). A site 2.5 kb upstream from the *Gapdhs* gene TSS was used as the internal control, and fold of enrichment was calculated using the $2^{\Delta Ct}$ method. The real-time PCR primers are listed in Supplemental Table S7.

For ChIP-seq, purified DNA was prepared for sequencing on a Beckman Coulter SPRI-TE following manufacturer's instructions. The seq-prepped DNA was PCR amplified using Illumina primers for 18 cycles. Samples were sequenced on either the Illumina Genome Analyzer II or Illumina Hi-Seq 2000 following the manufacturer's protocols. Raw ChIP-Seq

data were processed using the Illumina software pipeline. Only ChIP-Seq reads that aligned to exactly one location in the reference mouse genome (UCSC, mm9) were retained. See Supplemental Experimental Procedures for data analysis details.

RNA interference, quantitative RT-PCR and cDNA microarray analysis

Validated shRNA clones in the pLKO.1-puro vector (TRCN0000084942 (CBFβ), TRCN0000040581 (Ring1b) and TRCN00000257390 (Ring1b)) were obtained from Sigma-Aldrich, and the empty vector was used as control. Twenty-four hours after infection, cells were washed twice with phosphate buffered saline (PBS) and fresh medium was added. Forty-eight hours after transduction, puromycin (2 μg/ml final conc.) and TPA (50 ng/ml final conc.) were added. The cells were cultured for another 72 hrs before harvest and analyzed by qRT-PCR or cDNA microarray. The qRT-PCR primers are listed in Supplemental Figure S7.

Zebrafish maintenance and morpholino microinjection

See Supplemental Experimental Procedures.

Accession numbers

The ChIP-seq and cDNA microarray data have been deposited in the Gene Expression Omnibus public database under accession numbers GSE33653 and GSE33659, respectively. All animal procedures were approved by the Children's Hospital Institutional Animal Care and Use Committee.

Supplementary Material

Refer to Web version on PubMed Central for supplementary material.

Acknowledgments

M.Y. is supported by a grant from the Wendy Will Case Cancer Fund and an American Heart Association post-doctoral fellowship award. A.B.C. is supported by a grant from the NIH (R01-HL082952). E.F. is the recipient of the Eugene Bell Career Development Chair. This work used computing resources funded by the National Science Foundation under Award No. DB1-0821391, and sequencing support from the NIH (P30-ES002109). The authors would like to thank D. Gary Gilliland, Stuart Orkin, and Maarten van Lohuizen for providing knock out mouse strains, and Ross Tomaino and Steven Gygi at the Taplin Mass Spectrometry Facility for assistance with protein identification.

References

Appleford PJ, Woollard A. RUNX genes find a niche in stem cell biology. J Cell Biochem. 2009; 108:14–21. [PubMed: 19562739]

Bakshi R, Hassan MQ, Pratap J, Lian JB, Montecino MA, van Wijnen AJ, Stein JL, Imbalzano AN, Stein GS. The human SWI/SNF complex associates with RUNX1 to control transcription of hematopoietic target genes. J Cell Physiol. 2010; 225:569–576. [PubMed: 20506188]

Bejar R, Stevenson K, Abdel-Wahab O, Galili N, Nilsson B, Garcia-Manero G, Kantarjian H, Raza A, Levine RL, Neuberg D, Ebert BL. Clinical effect of point mutations in myelodysplastic syndromes. N Engl J Med. 2011; 364:2496–2506. [PubMed: 21714648]

Burns CE, DeBlasio T, Zhou Y, Zhang J, Zon L, Nimer SD. Isolation and characterization of runxa and runxb, zebrafish members of the runt family of transcriptional regulators. Exp Hematol. 2002; 30:1381–1389. [PubMed: 12482499]

Burns CE, Traver D, Mayhall E, Shepard JL, Zon LI. Hematopoietic stem cell fate is established by the Notch-Runx pathway. Genes Dev. 2005; 19:2331–2342. [PubMed: 16166372]

Cales C, Roman-Trufero M, Pavon L, Serrano I, Melgar T, Endoh M, Perez C, Koseki H, Vidal M. Inactivation of the polycomb group protein Ring1B unveils an antiproliferative role in

hematopoietic cell expansion and cooperation with tumorigenesis associated with Ink4a deletion. Mol Cell Biol. 2008; 28:1018–1028. [PubMed: 18039844]

Chen MJ, Yokomizo T, Zeigler BM, Dzierzak E, Speck NA. Runx1 is required for the endothelial to haematopoietic cell transition but not thereafter. Nature. 2009; 457:887–891. [PubMed: 19129762]

Dennis G Jr. Sherman BT, Hosack DA, Yang J, Gao W, Lane HC, Lempicki RA. DAVID: Database for Annotation, Visualization, and Integrated Discovery. Genome Biol. 2003; 4:P3. [PubMed: 12734009]

Drachman JG, Sabath DF, Fox NE, Kaushansky K. Thrombopoietin signal transduction in purified murine megakaryocytes. Blood. 1997; 89:483–492. [PubMed: 9002950]

Elagib KE, Racke FK, Mogass M, Khetawat R, Delehanty LL, Goldfarb AN. RUNX1 and GATA-1 coexpression and cooperation in megakaryocytic differentiation. Blood. 2003; 101:4333–4341. [PubMed: 12576332]

Eng JK, McCormack AL, Yates JR III. An approach to correlate tandem mass spectral data of peptides with amino acid sequences in a protein database. J. Am. Soc. Mass Spectrom. 1994; 5:976–989.

Galli C, Fu Q, Wang W, Olsen BR, Manolagas SC, Jilka RL, O'Brien CA. Commitment to the osteoblast lineage is not required for RANKL gene expression. J Biol Chem. 2009; 284:12654–12662. [PubMed: 19279010]

Georgiades P, Ogilvy S, Duval H, Licence DR, Charnock-Jones DS, Smith SK, Print CG. VavCre transgenic mice: a tool for mutagenesis in hematopoietic and endothelial lineages. Genesis. 2002; 34:251–256. [PubMed: 12434335]

Growney JD, Shigematsu H, Li Z, Lee BH, Adelsperger J, Rowan R, Curley DP, Kutok JL, Akashi K, Williams IR, et al. Loss of Runx1 perturbs adult hematopoiesis and is associated with a myeloproliferative phenotype. Blood. 2005; 106:494–504. [PubMed: 15784726]

Guo Y, Papachristoudis G, Altshuler RC, Gerber GK, Jaakkola TS, Gifford DK, Mahony S. Discovering homotypic binding events at high spatial resolution. Bioinformatics. 2010; 26:3028–3034. [PubMed: 20966006]

Huang G, Zhang P, Hirai H, Elf S, Yan X, Chen Z, Koschmieder S, Okuno Y, Dayaram T, Growney JD, et al. PU.1 is a major downstream target of AML1 (RUNX1) in adult mouse hematopoiesis. Nat Genet. 2008; 40:51–60. [PubMed: 17994017]

Huang H, Yu M, Akie TE, Moran TB, Woo AJ, Tu N, Waldon Z, Lin YY, Steen H, Cantor AB. Differentiation-dependent interactions between RUNX-1 and FLI-1 during megakaryocyte development. Mol Cell Biol. 2009; 29:4103–4115. [PubMed: 19470763]

Ichikawa M, Asai T, Saito T, Yamamoto G, Seo S, Yamazaki I, Yamagata T, Mitani K, Chiba S, Hirai H, et al. AML-1 is required for megakaryocytic maturation and lymphocytic differentiation, but not for maintenance of hematopoietic stem cells in adult hematopoiesis. Nat Med. 2004; 10:299–304. [PubMed: 14966519]

Jacob B, Osato M, Yamashita N, Wang CQ, Taniuchi I, Littman DR, Asou N, Ito Y. Stem cell exhaustion due to Runx1 deficiency is prevented by Evi5 activation in leukemogenesis. Blood. 2010; 115:1610–1620. [PubMed: 20008790]

Kim WY, Sieweke M, Ogawa E, Wee HJ, Englmeier U, Graf T, Ito Y. Mutual activation of Ets-1 and AML1 DNA binding by direct interaction of their autoinhibitory domains. Embo J. 1999; 18:1609–1620. [PubMed: 10075931]

Kissa K, Herbomel P. Blood stem cells emerge from aortic endothelium by a novel type of cell transition. Nature. 2010; 464:112–115. [PubMed: 20154732]

Lin HF, Traver D, Zhu H, Dooley K, Paw BH, Zon LI, Handin RI. Analysis of thrombocyte development in CD41-GFP transgenic zebrafish. Blood. 2005; 106:3803–3810. [PubMed: 16099879]

MacIsaac KD, Lo KA, Gordon W, Motola S, Mazor T, Fraenkel E. A quantitative model of transcriptional regulation reveals the influence of binding location on expression. PLoS Comput Biol. 2010; 6:e1000773. [PubMed: 20442865]

Margueron R, Reinberg D. The Polycomb complex PRC2 and its mark in life. Nature. 2011; 469:343–349. [PubMed: 21248841]

Mohd-Sarip A, van der Knaap JA, Wyman C, Kanaar R, Schedl P, Verrijzer CP. Architecture of a polycomb nucleoprotein complex. Mol Cell. 2006; 24:91–100. [PubMed: 17018295]

Motoda L, Osato M, Yamashita N, Jacob B, Chen LQ, Yanagida M, Ida H, Wee HJ, Sun AX, Taniuchi I, et al. Runx1 protects hematopoietic stem/progenitor cells from oncogenic insult. Stem Cells. 2007; 25:2979–2986.

North T, Gu TL, Stacy T, Wang Q, Howard L, Binder M, Marin-Padilla M, Speck NA. Cbfa2 is required for the formation of intra-aortic hematopoietic clusters. Development. 1999; 126:2563–2575. [PubMed: 10226014]

Park IK, Qian D, Kiel M, Becker MW, Pihalja M, Weissman IL, Morrison SJ, Clarke MF. Bmi-1 is required for maintenance of adult self-renewing haematopoietic stem cells. Nature. 2003; 423:302–305. [PubMed: 12714971]

Pasini D, Bracken AP, Hansen JB, Capillo M, Helin K. The polycomb group protein Suz12 is required for embryonic stem cell differentiation. Mol Cell Biol. 2007; 27:3769–3779. [PubMed: 17339329]

Schoeftner S, Sengupta AK, Kubicek S, Mechtler K, Spahn L, Koseki H, Jenuwein T, Wutz A. Recruitment of PRC1 function at the initiation of X inactivation independent of PRC2 and silencing. Embo J. 2006; 25:3110–3122. [PubMed: 16763550]

Setoguchi R, Tachibana M, Naoe Y, Muroi S, Akiyama K, Tezuka C, Okuda T, Taniuchi I. Repression of the transcription factor Th-POK by Runx complexes in cytotoxic T cell development. Science. 2008; 319:822–825. [PubMed: 18258917]

Simon JA, Kingston RE. Mechanisms of polycomb gene silencing: knowns and unknowns. Nat Rev Mol Cell Biol. 2009; 10:697–708. [PubMed: 19738629]

Song WJ, Sullivan MG, Legare RD, Hutchings S, Tan X, Kufrin D, Ratajczak J, Resende IC, Haworth C, Hock R, et al. Haploinsufficiency of CBFA2 causes familial thrombocytopenia with propensity to develop acute myelogenous leukaemia. Nat Genet. 1999; 23:166–175. [PubMed: 10508512]

Speck NA, Gilliland DG. Core-binding factors in haematopoiesis and leukaemia. Nat Rev Cancer. 2002; 2:502–513. [PubMed: 12094236]

Sun W, Downing JR. Haploinsufficiency of AML1 results in a decrease in the number of LTR-HSCs while simultaneously inducing an increase in more mature progenitors. Blood. 2004; 104:3565–3572. [PubMed: 15297309]

Talebian L, Li Z, Guo Y, Gaudet J, Speck ME, Sugiyama D, Kaur P, Pear WS, Maillard I, Speck NA. T-lymphoid, megakaryocyte, and granulocyte development are sensitive to decreases in CBFbeta dosage. Blood. 2007; 109:11–21. [PubMed: 16940420]

van der Lugt NM, Domen J, Linders K, van Roon M, Robanus-Maandag E, te Riele H, van der Valk M, Deschamps J, Sofroniew M, van Lohuizen M, et al. Posterior transformation, neurological abnormalities, and severe hematopoietic defects in mice with a targeted deletion of the bmi-1 proto-oncogene. Genes Dev. 1994; 8:757–769. [PubMed: 7926765]

Villeval JL, Cohen-Solal K, Tulliez M, Giraudier S, Guichard J, Burstein SA, Cramer EM, Vainchenker W, Wendling F. High thrombopoietin production by hematopoietic cells induces a fatal myeloproliferative syndrome in mice. Blood. 1997; 90:4369–4383. [PubMed: 9373248]

Vincenz C, Kerppola TK. Different polycomb group CBX family proteins ssociate with distinct regions of chromatin using nonhomologous protein sequences. Proc Natl Acad Sci U S A. 2008; 105:16572–16577. [PubMed: 18927235]

Walrad PB, Hang S, Joseph GS, Salas J, Gergen JP. Distinct Contributions of Conserved Modules to Runt Transcription Factor Activity. Mol Biol Cell. 2010; 21:2315–2326. [PubMed: 20462957]

Wang Q, Stacy T, Binder M, Marin-Padilla M, Sharpe AH, Speck NA. Disruption of the Cbfa2 gene causes necrosis and hemorrhaging in the central nervous system and blocks definitive hematopoiesis. Proc Natl Acad Sci U S A. 1996a; 93:3444–3449. [PubMed: 8622955]

Wang Q, Stacy T, Miller JD, Lewis AF, Gu TL, Huang X, Bushweller JH, Bories JC, Alt FW, Ryan G, et al. The CBFbeta subunit is essential for CBFalpha2 (AML1) function in vivo. Cell. 1996b; 87:697–708. [PubMed: 8929538]

Wilson BG, Wang X, Shen X, McKenna ES, Lemieux ME, Cho YJ, Koellhoffer EC, Pomeroy SL, Orkin SH, Roberts CW. Epigenetic antagonism between polycomb and SWI/SNF complexes during oncogenic transformation. Cancer Cell. 2011; 18:316–328. [PubMed: 20951942]

Wilson NK, Foster SD, Wang X, Knezevic K, Schutte J, Kaimakis P, Chilarska PM, Kinston S, Ouwehand WH, Dzierzak E, et al. Combinatorial transcriptional control in blood stem/progenitor

cells: genome-wide analysis of ten major transcriptional regulators. Cell Stem Cell. 2010; 7:532–544. [PubMed: 20887958]

Woo CJ, Kharchenko PV, Daheron L, Park PJ, Kingston RE. A region of the human HOXD cluster that confers polycomb-group responsiveness. Cell. 2010; 140:99–110. [PubMed: 20085705]

Yu M, Riva L, Xie H, Schindler Y, Moran TB, Cheng Y, Yu D, Hardison R, Weiss MJ, Orkin SH, et al. Insights into GATA-1-mediated gene activation versus repression via genome-wide chromatin occupancy analysis. Mol Cell. 2009; 36:682–695. [PubMed: 19941827]

Yu M, Wan M, Zhang J, Wu J, Khatri R, Chi T. Nucleoprotein structure of the CD4 locus: implications for the mechanisms underlying CD4 regulation during T cell development. Proc Natl Acad Sci U S A. 2008; 105:3873–3878. [PubMed: 18322012]

Zhang Y, Liu T, Meyer CA, Eeckhoute J, Johnson DS, Bernstein BE, Nusbaum C, Myers RM, Brown M, Li W, Liu XS. Model-based analysis of ChIP-Seq (MACS). Genome Biol. 2008; 9:R137. [PubMed: 18798982]

Zhao J, Sun BK, Erwin JA, Song JJ, Lee JT. Polycomb proteins targeted by a short repeat RNA to the mouse X chromosome. Science. 2008; 322:750–756. [PubMed: 18974356]

Highlights

- PRC1 interacts with Runx1 and CBFβ
- PRC1 and Runx1/CBFβ co-localize on chromatin and co-regulate a subset of genes
- PRC1 and Runx1/CBFβ deficiency generate partial phenocopies of one another *in vivo*
- Runx1 directly recruits PRC1 independent of PRC2

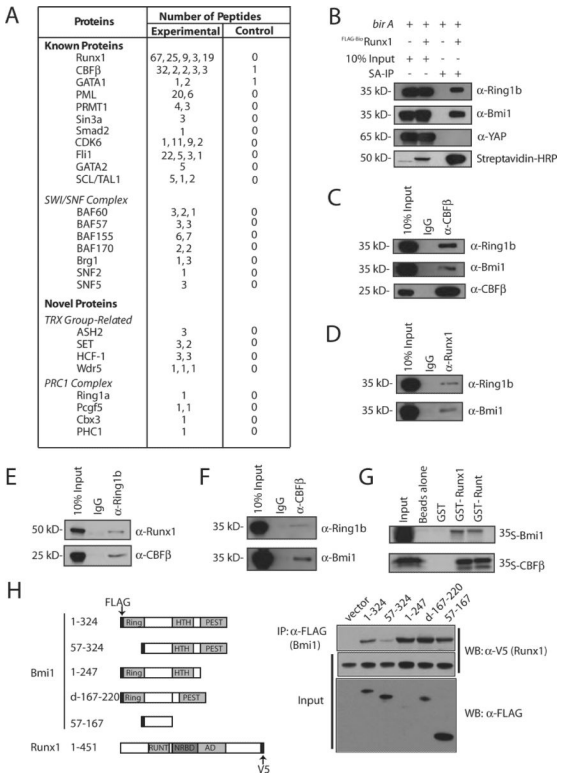

Figure 1.

Physical association between Runx1/CBFβ and Ring1b/Bmi1. (A) Partial list of proteins identified by mass spectrometry following tandem anti-FLAG:SA or single SA affinity chromatography from crude nuclear extracts of $^{FLAG\text{-}Bio}$Runx1 + biotin ligase *birA* (experimental) or *birA* alone (control) containing L8057 cells treated with TPA for 72 hrs (Huang et al., 2009). The number of peptides obtained for each protein from each of 5 independent experiments is shown. See Supplemental Figure S1 and Supplemental Table S1 for additional details. (B) Western blot for Ring1b, Bmi1 and YAP following SA-IP of $^{FLAG\text{-}Bio}$Runx1 complexes from TPA-induced L8057 cells. Ten percent input is shown. (C–E) Co-IP assays of endogenous proteins from TPA-induced L8057 cells. The IP antibody is shown on top, and the WB antibody is shown on the right. Ten percent input is shown. IgG, species matched control antibody. (F) Western blot for Ring1b and Bmi1 following IP with α-CBFβ antibody, or control IgG, from Jurkat T cells. Ten percent input is shown. (G) GST pull-down assay of recombinant Runx1, Bmi1 and CBFβ. *In vitro* transcribed and translated [^{35}S]-methionine labeled Bmi1 or CBFβ was incubated with uncoupled beads or beads coupled with GST, GST-Runx1 or GST-runt domain fusion proteins as indicated. The beads were washed and eluted material was separated by SDS-PAGE. An autoradiogram is shown. Ten percent of the input protein is shown. (H) Mapping of Bmi1 interaction domain. Left, schematic diagram of constructs. Right, α-FLAG IP followed by α-V5 Western blot of constructs co-expressed in COS7 cells. One percent of input is shown.

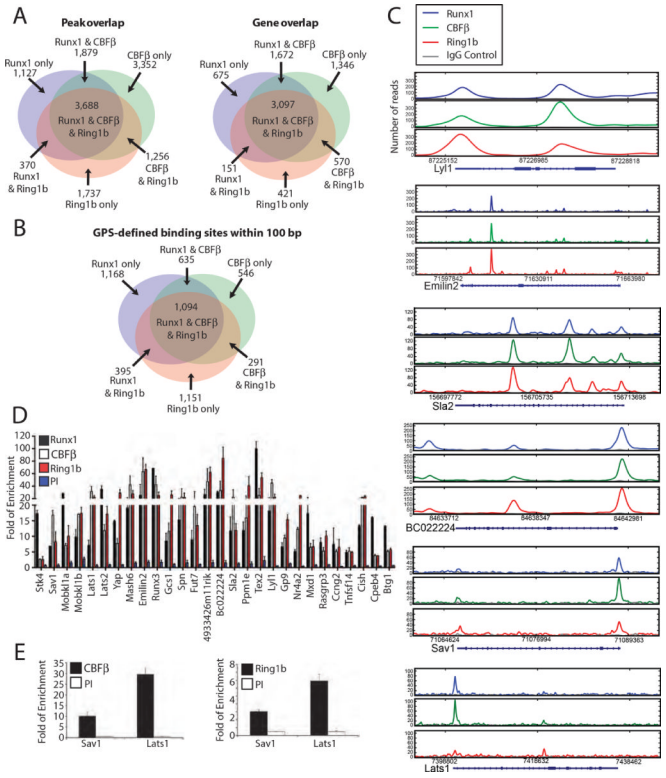

Figure 2.

Common chromatin site occupancy by Runx1/CBFβ and Ring1b. (A) Venn diagrams showing overlap of Runx1, CBFβ, and Ring1b occupancy peaks (left) and genes (right) in TPA-induced L8057 cells based on MACS (Zhang et al., 2008). Overlapping peaks are defined as those for which the summits of the peaks are < 500 bp from each other. Bound genes are defined as having occupancy peaks between −1kb of the TSS to +1kb of the TES. (B) Venn diagram showing overlap of Runx1, CBFβ, and Ring1b occupancy sites within 100 bp of one another based on GPS (Guo et al., 2010). (C) Representative Runx1, CBFβ, Ring1b, and control IgG ChIP-seq profiles of loci occupied by Runx1, CBFβ and Ring1b. Other genes present in these regions are not shown. (D) qChIP assays for Runx1, CBFβ and Ring1b occupancy at the indicated loci in TPA-induced L8057 cells. PI, control antibody. The data is expressed as fold enrichment relative to a negative control region (−2.5 kb 5' of the *Gapdhs* gene TSS), and represent the mean of 3 independent experiments ± standard deviation (std dev). (E) qChIP assays for CBFβ and Ring1b occupancy at *Sav1* and *Lats1* gene promoters in primary fetal liver derived murine Mks. The data are displayed as in “D”.

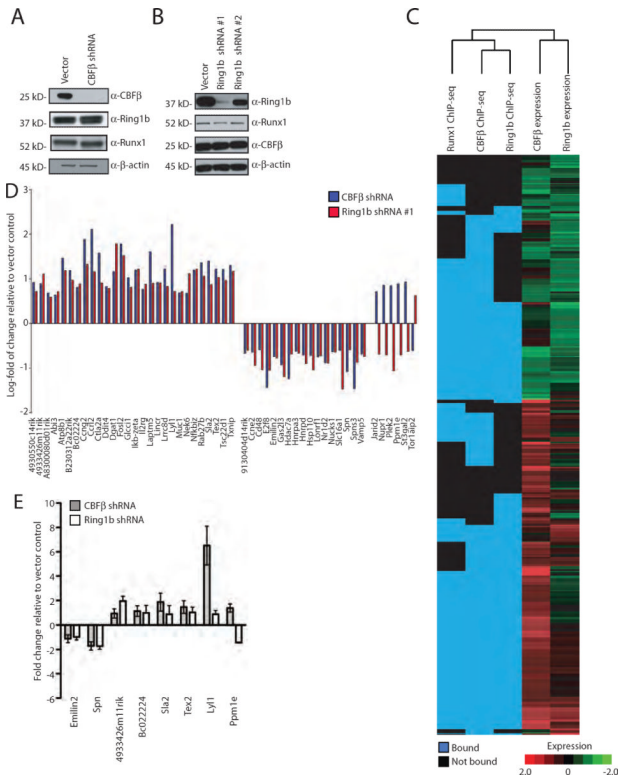

Figure 3.

Regulation of a subset of commonly bound CBFβ and Ring1b direct target genes. (A) CBFβ lentiviral shRNA knock down in TPA-induced L8057 cells. Western blot for CBFβ, Ring1b, Runx1, and β-actin in puromycin selected cells. (B) Ring1b lentiviral shRNA knock down in TPA-induced L8057 cells. Western blot for Ring1b, Runx1, CBFβ and β-actin in puromycin selected cells. (C) Clustering analysis showing genes occupied by either Runx1, CBFβ and/or Ring1b at −1kb of TSS to +1kb of TES, and heat map of corresponding gene expression changes (red, increased; green, decreased; black, no change) following CBFβ or Ring1b shRNA knock down. (D) Log-fold gene expression changes based on cDNA microarray analysis for genes bound by at all 3 factors (Runx1, CBFβ, and Ring1b) (p-value <1E-10, FDR < 5%; occupancy −1kb of the TSS to +1 kb from the TES) that changed expression following bothβ and Ring1b shRNA knock down ≥ 1.5 fold with p-value < 0.05. (E) qRT-PCR measurements of gene expression changes of representative commonly occupied genes following CBFβ or Ring1b shRNA knock down in TPA-induced L8057 cells. Levels are normalized to Gapdhs. The mean of 4 independent experiments is shown ± std dev.

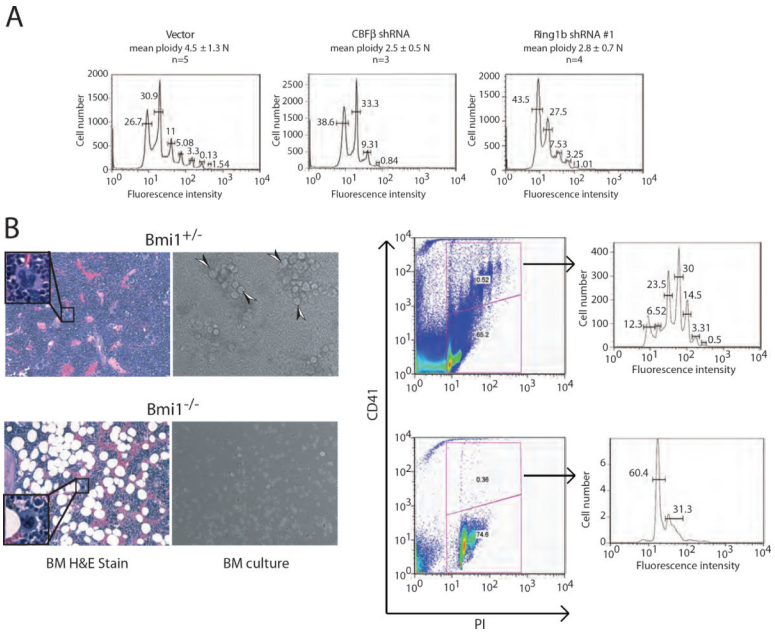

Figure 4.

Partial phenocopies of Ring1b/Bmi1 and Runx1/CBFβ deficiency in megakaryopoiesis. (A) Representative flow cytometric plots of propidium iodide (PI) DNA ploidy analysis of TPA-induced L8057 cells transduced with the empty vector, CBFβ shRNA, or Ring1b shRNA #1. The percentages of cells with each DNA ploidy state (2N, 4N, 16N, 32N, 64N and 128N) and the mean ploidy (vector (n=5), CBFb shRNA (n=3), Ring1b shRNA #1 (n=4)) are given ± std dev. (B) Phenotype of $Bmi1^{-/-}$ Mks. Left panel, hematoxylin and eosin stained histologic sections of bone marrow from $Bmi1^{+/-}$ mice. Inset shows representative Mk at higher magnification (original 600×). Middle panel, phase contrast photomicrograph of bone marrow cells cultured from $Bm1^{+/-}$ and $Bmi1^{-/-}$ mice in the presence Tpo and stem cell factor. Arrowheads indicate large (maturing) Mks. Right panel, flow cytometric plots of cultured bone marrow cells for CD41 expression and DNA content (PI). Histogram plots for different ploidy classes are shown to the right for $CD41^{+}$ gated cells. Gates were set using control IgG stained cells.

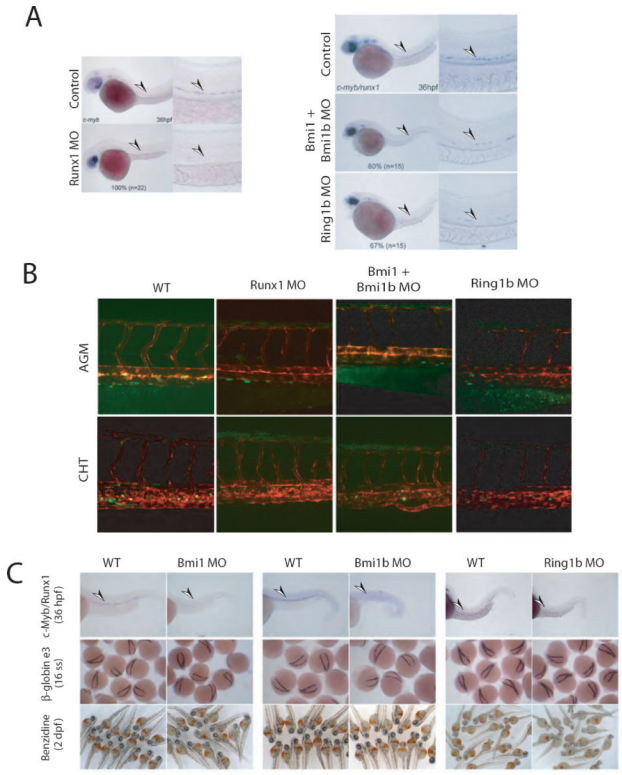

Figure 5.

Partial phenocopies of Ring1b/Bmi1 and Runx1/CBFβ deficiency in definitive HSC ontogeny. (A) Left panel, *in situ* hybridization for *c-Myb* in 36 hours post fertilization (hpf) uninjected control and *Runx1* morphant zebrafish embryos. Low magnification (10×) (left) and high magnification (40×) images of the trunk region (right) are shown. MO, morpholino. The percentage of embryos with the represented phenotype is indicated. Right panel, *in situ* hybridization for *c-Myb/Runx1* in 36 hpf uninjected control or embryos injected at the single cell stage with *Bmi1*, *Bmi1b* and/or *Ring1b* translation blocking MOs. Arrowheads indicate phenotypic HSCs. (B) MO injection into transgenic CD41-eGFP: flk1-RFP double transgenic embryos. $eGFP^+$ cells (green) represent HSPCs and thrombocytes, RFP^+ cells (red) represent vasculature. The AGM region was visualized at 36 hpf, and the CHT was visualized 3 days later. (C) Upper row, *in situ* hybridization for c-Myb and Runx1 at 36 hrs hpf in zebrafish embryos injected with Bmi1, Bmi1b, or Ring1b MOs, compared to wild type (WT) embryos. Middle row, ε3-globin *in situ* hybridization at the 16-somite stage (ss). Lower row, o-dianosidine (benzidine) stains of 2 days post fertilization (dpf) embryos. Hemoglobinized cells stain orange/brown.

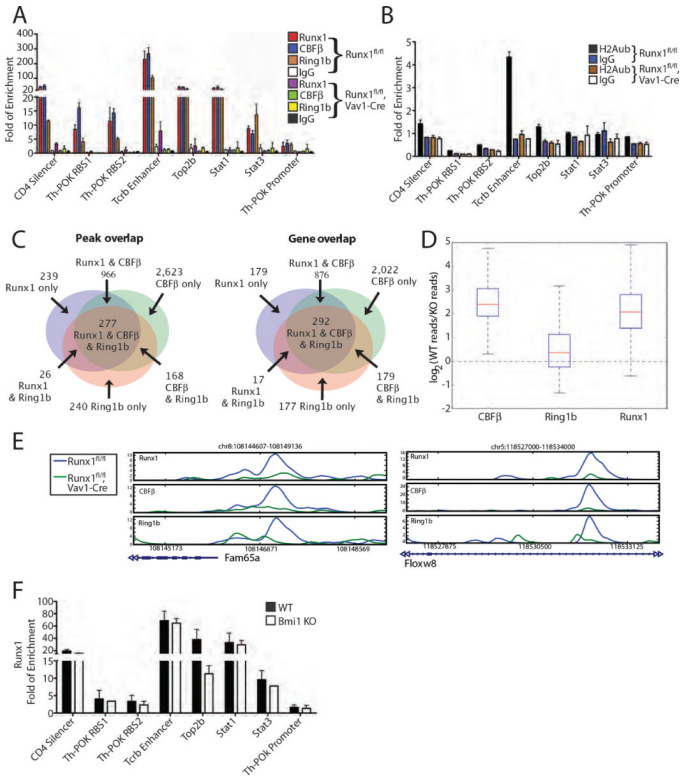

Figure 6.

Runx1 dependency of Ring1b chromatin occupancy at commonly bound sites in primary murine thymocytes. (A) qChIP assays for Runx1, CBFβ and Ring1b in primary thymocytes from either Runx1$^{fl/fl}$ or Runx1$^{fl/fl}$, Vav1-Cre 6-week old mice. Fold of enrichment is shown relative to a negative control region (see Methods). The mean of 3 independent assays is shown ± std dev. (B) qChIP assay for H2Aub at each of the individual sites tested in "A". (C) Venn diagrams showing overlap of Runx1, CBFβ and Ring1b peaks and bound genes from primary thymocytes of 5–8 week old Runx1$^{fl/fl}$ mice. Peaks are filtered for p-value < 1E-10, FDR < 5% and overlaps are defined as MACS summits within 500 bp of each other. Bound genes contain occupancy peaks within −1kb of the TSS to + 1kb of the TES. (D) Ratio of the number of reads obtained from ChIP-seq for CBFβ, Ring1b, and Runx1 at commonly occupied sites in thymocytes from Runx1$^{fl/fl}$ versus Runx1$^{fl/fl}$, Vav1-Cre mice in log-base-2. The red horizontal bars represent the median value, the boxes represent the 25th–75th%ile range, and the whiskers extend to the most extreme data point within 1.5× of the inner quartile. The expected log-ratios based on the number of reads in each experiment are −0.29 for CBFβ, −0.51 for Ring1b, and 0.25 for Runx1. (E) Examples of ChIP-seq profiles showing concomitant reduction of Runx1, CBFβ and Ring1b occupancy at commonly occupied sites. (F) qChIP assays for Runx1 in primary thymocytes from 5–6 week old Bmi1$^{-/-}$ or wild type littermate controls. The mean of 3 independent assays is shown ± std dev.

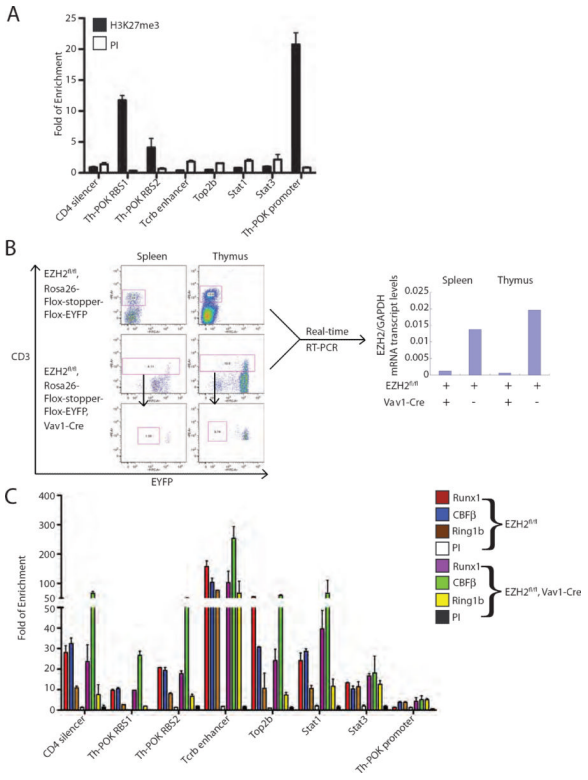

Figure 7.

PRC2 independent occupancy of Ring1b at Runx1/CBFβ commonly occupied genes. (A) qChIP assays for H3K27me3 at each of the indicated sites in wild type murine primary thymocytes. The mean of 3 independent assays is shown ± std dev. (B) Left panel, flow cytometry for CD3 and EYFP expression from spleen or thymus of EZH2$^{fl/fl}$, Rosa26-flox-stopper-flox-EYFP and EZH2$^{fl/fl}$, Rosa26-flox-stopper-flox-EYFP, Vav1-Cre mice. Right panels, qRT-PCR analysis for EZH2 mRNA transcript levels in corresponding splenic or thymic CD3^{+} cells. (C) qChIP assays for Runx1, CBFβ and Ring1b in primary thymocytes from 6–8 week old EZH2$^{fl/fl}$, Rosa26-flox-stopper-flox-EYFP or EZH2$^{fl/fl}$, Rosa26-flox-stopper-flox-EYFP, Vav1-Cre littermates. The data is expressed as fold enrichment relative to a negative control region (see Methods). The data represent the mean of 3 independent experiments for Ring1b, and 2 independent experiments for Runx1 and CBFb ± std. dev.